Experimental Study and Finite Element Analysis of Composite Constrained Concrete With Steel Tube and Prestressed Steel Hoop

Depeng Wang[1],and Yikang Li[2], and Dan Zhang[3*] Yafei Zhang[4,5]

[1] Xingrun Construction Group Co., LTD, Shandong, Feicheng, 271600, China,
[2] China Construction Sixth Engineering Bureau Corp., Ltd, Tianjin 300012, China.
[3] School of Civil and Transportation Engineering, Hebei University of Technology, Tianjin 300401, China.
[4]School of Civil Engineering, Tianjin University, Tianjin 300350, China
[5]School of Engineering & Built Environment, Griffith University, Gold Coast Campus, Queensland 4222, Australia
zd951767323@tju.edu.cn

Abstract. To study the axial compression performance of composite constrained concrete columns with steel tube and prestressed steel hoops, seven groups (three specimens each group) were subjected to axial compression tests of constrained concrete columns. The axial compression mechanism of steel tube and prestressed steel hoop composite constrained specimens is analyzed from the destruction pattern of the specimen, the destruction pattern of external prestressed steel hoop, load-displacement curve and load-strain curve. And compared with steel tube or prestressed steel hoop alone constrained concrete column. The axial stress performance of composite constrained concrete columns was analyzed by finite element software ABAQUS. The results show that the steel tube and prestressed steel hoop composite constrained concrete have better bearing capacity and deformation capacity compared with steel tube or prestressed steel hoop alone constrained concrete column. As the prestressed steel hoop increases in prestressing level and the spacing decreases, its bearing capacity also increases. The load-strain curve of the established model agrees well with the test. Therefore, it is feasible to analyze the axial compression of the composite constrained concrete by using the ABAQUS finite element model established in this paper.

Keywords: Steel jackets reinforced concrete, Prestressed steel hoop, constrained concrete, Axial compression, Finite element analysis

1 Introduction

The main limitation of the concrete, which is the most commonly used building material, lies in its brittle failure form that offers little warning before failure occurs. Enhancing the lateral constraint of concrete serves as a common approach to enhance both its strength and ductility. Concrete lateral restraint can be categorized into

W. Guo et al. (eds.), *Proceedings of the 3rd International Conference on Green Building, Civil Engineering and Smart City (GBCESC 2024)*, Advances in Engineering Research 264,
https://doi.org/10.2991/978-94-6463-728-1_10

passive and active types based on the different methods employed for applying lateral restraint pressure [1]. The key distinction between these two types of constraints lies in the fact that lateral pressure exists prior to subjecting concrete to axial load. In passive restrained concrete, this lateral pressure arises from concrete expansion and is accompanied by concomitant damage.

Theoretical analysis and experimental research have been extensively conducted by both domestic and foreign scholars on passive restrained concrete. Various methods for achieving passive restraint, such as stirrup restrained concrete, steel tube restrained concrete, and fiber reinforced composite material (FRP) restrained concrete, have been investigated. It has been found that the bearing capacity of restrained concrete members can be effectively improved with an increase in steel content [3-6]. However, studies indicate that when the steel ratio is low, the restraint effect of a steel tube on concrete is relatively poor, resulting in overall shear failure of the concrete filled steel tube. To avoid this shear destruction pattern in constrained fiber-reinforced cementitious composites (CFST), increasing the wall thickness of the steel tube is necessary. Nevertheless, this leads to an increase in section area and mass as well as stiffness (primarily flexural stiffness) of CFST components. Consequently, it reduces their natural vibration period and increases seismic demand [7]. Furthermore, it should be noted that a steel tube only exerts a restraining effect on core concrete when subjected to axial loads close to its yield load and radial expansion-induced circumferential stress within the tube [8], which also introduces stress lag issues .

There is a limited body of research on actively restrained concrete, with existing studies predominantly concentrating on Shape Memory Alloy (SMA) restrained concrete and prestressed steel strand restrained concrete. Research [9][10] indicates that concrete constrained by Shape Memory Alloys (SMA) and prestressed steel strands can provide effective initial horizontal restraint under load, addressing stress lag issues. However, it is important to note that if the constrained concrete is damaged, both SMA and prestressed steel strands may penetrate the concrete, leading to stress loss. Additionally, active restraint technology is relatively complex, requiring substantial manpower, mechanical equipment, and resources, which can be time-consuming and costly. Fakharifar[11] proposed a method combining thin steel plates with prestressed steel strands to strengthen piers in order to address stress loss because of concrete penetration during seismic repairs and increased structural seismic demands during pier repair and reinforcement using thick steel plates. The results turn out that this method can restore the bearing capacity and ductility of piers even beyond their original levels while achieving satisfactory repair effects. Nevertheless, challenges remain such as the need for tensioning prestressed steel strands using mechanical equipment and additional manpower.

In this study, based on Fakharifar's research, the combination of stainless steel plate and prestressed steel hoop is used to restrain concrete together to form a mixed restraint form. The active constraint of prestressed steel hoops can solve the problem of passive constraint stress hysteresis well, and the existence of steel plates can retain the prestressed stress well without penetrating the concrete and causing stress loss, and can effectively constrain the bearing capacity and ductility of concrete. Based on the proposed mixed restraint form, this study performed axial compression tests on 21 concrete specimens, including both unrestrained concrete and steel tube-restrained concrete, prestressed steel hoop-restrained concrete and mixed restrained concrete specimens. The composite restraint specimens of steel hoops and prestressed steel hoops were analyzed from the aspects of load-displacement curve and load-strain curve of the specimens. On the basis of the experimental research, the finite element analysis software ABAQUS is used to simulate the axial pressure performance of the composite constrained concrete specimen, and then promote the further research and application of the composite constrained concrete specimen.

2 Test profile

2.1 Specimen design

A total of twenty-one 150mm × 300mm concrete cylinders were designed in this experiment. The influences of three factors on the axial static properties of the specimens were considered: different constraint types (unconstrained, active, passive and mixed constraints), the distance between the wires of the steel hooped (145mm,97mm) and different prestress levels (0.3 and 0.4 times tensile strength). Detailed design parameters of specimens are shown in Table 1. In Table 1, h is the restrained height of the steel plate, S is the distance between the middle lines of the steel hoop, and k is the initial prestress level of the steel hoop.

The specimen preparation involves two main steps: forming the plain concrete cylinders and applying external constraints. Initially, plain concrete cylinders are cast alongside a batch of cube and prism test blocks, which are cured under standard conditions for 28 days. The active constraint utilizes prestressed steel hoops specifically, 1 mm thick and 26 mm wide 201 stainless steel hoops applied to the concrete. The passive constraint employs 1 mm thick stainless steel plates, which are welded to the specimen. For mixed constraints, the process involves wrapping the concrete with a steel pipe and then applying prestressed steel hoops over the pipe. When using the steel plate as an external constraint, the thin stainless steel plate is attached to the concrete cylinder with the steel hoop, ensuring a tight fit with no gaps. The lower edge of the plate is aligned with the bottom of the concrete specimen, while the upper edge is positioned 10 mm below the top of the specimen (except for Group S samples, where it is flush with the concrete height). The steel plate is then spot-welded in place, and after securing the connection, the steel hoop is removed before welding the outer steel pipe.

Table 1. Specimen number and parameters

Number	Constrain t type	Constraint quantity	h(mm)	S(mm)	k
PS-3-04-C1,C2,C3	Active	1 plate3 hoops	290	132	0.4
PS-3-03-C1,C2,C3	Active	1 plate3 hoops	290	132	0.3

PS-4-03-C1,C2,C3	Active	1 plate3 hoops	290	88	0.3
P-C1,C2,C3	Active	3 hoops	-	132	None
UC-C1,C2,C3	None	None	-	-	None
S-C1,C2,C3	Passive	1 plate	300	-	None
SC-C1,C2,C3	Passive	1 plate	290	-	None

The method for applying prestress to the steel hoop is as follows: The steel hoop, connected to the strain measuring instrument, is positioned around the outside of the specimen. The bolt is then turned to secure the steel hoop to the specimen, and the strain of the collector is set to zero. The bolt is further tightened to apply the initial prestress. The prestress application is divided into four stages—20%, 50%, 80%, and 100% of the design value. At each stage, prestress is first applied to the middle section of the steel band and then to the ends until the strain measured by the collector reaches the specified design initial strain value.

2.2 Material properties

The concrete used in the test was C40 concrete, and the same batch of 100mm side length concrete cube test blocks and 100mm×100mm×300mm prismatic test blocks were reserved during the pouring of the specimens. They were maintained by standard, and their compressive strength and elastic modulus were tested according to the Standard of Test Method for Mechanical Properties of Ordinary Concrete [13]. The cubic compressive strength f_{cu}=43.3MPa, the axial compressive strength f_{cp}=31.6MPa, and the elastic modulus E=35.7GPa were obtained.

The stainless steel plate and the prestressed steel hoop are both 201 stainless steel, and the tensile test is carried out according to the method given in the code "Tensile Test of Metal Materials" [12]. The results are shown in Table 2.In the Table 2, t, E, f_y and f_u are respectively the thickness, elastic modulus, yield strength and ultimate strength of stainless steel materials.

Table 2. Steel material properties

Type	t(mm)	E(MPa)	f_y(MPa)	f_u(MPa)
Stainless Steel plate	1.00	203400	346.15	618.36
Stainless Steel hoop	1.00	207600	334.33	637.25

2.3 Measurement scheme and loading system

For both unconstrained and actively constrained concrete specimens, two axial strain gauges and two circumferential BX120-50AA strain gauges are positioned 180 ° apart at the mid-height of the specimens to measure longitudinal and transverse strains, respectively. Additionally, for specimens subjected to initial prestress, two BX120-5AA strain gauges, also spaced 180 ° apart, are symmetrically placed to measure tensile strain. In the case of stainless steel constrained specimens, four circumferential and four axial strain gauges, all BX120-10AA, are installed at the mid-height, with each gauge arranged 90° apart to ensure comprehensive strain measurement. The layout of the Concrete-Filled Steel Tube (CFST) configuration is illustrated in Fig. 1. For lateral displacement, measurement points are located at the middle of the specimen, with two sensors positioned 180° apart. Vertical displacement is assessed by directing the laser onto an L-shaped steel sheet attached to the upper end of the specimen.

The electro-hydraulic servo 20t pressure testing machine produced by Jinan Times Testing Institute was used for monotonic loading. In order to avoid the uneven surface caused by the concrete curing process, fine sand is evenly laid at the bottom of the specimen to avoid stress concentration and premature damage caused by the uneven bottom surface. A circular loading plate is placed on the top of the specimen to make the load evenly applied. Before placing the circular loading plate, the specimen is centered and placed under eccentric compression. During the loading process, the specimen was controlled by force before reaching 200kN and the loading rate was 0.5kN/min, and then by displacement control and the loading rate was 1mm/min until the end of the test. Fig.2 presents the test setup.

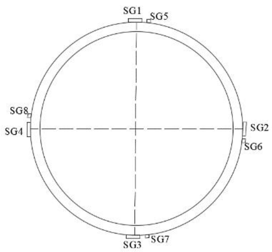

Fig. 1. Schematic diagram of strain gauge layout

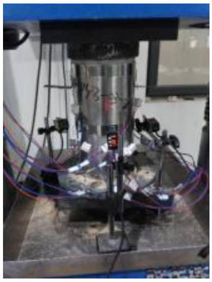

Fig. 2. Test set up

3 Main test results

3.1 Load-displacement curve

The load-displacement curves illustrated in Fig. 3 display variations in different hoop-spacing, initial prestress levels, and forms of constraint. Analysis of these curves reveals that increasing the prestress levels and reducing the spacing enhances the bearing capacity. Furthermore, it is observed that unrestrained concrete, characterized by poor ductility, exhibits low bearing capacity and a rapid decline in performance post-peak load, resulting in brittle failure. Conversely, actively restrained concrete, reinforced with prestressed steel hoops, demonstrates improved bearing capacity and ductility, though it still suffers from brittle failure. Notably, passively restrained concrete, utilizing steel tubes, shows significant improvements in both bearing capacity and ductility compared to unrestrained concrete. Additionally, mixed restrained concrete specimens, incorporating both steel tubes and prestressed steel hoops, exhibit a substantial increase in bearing capacity up to 60% and demonstrate excellent ductility. Therefore, it can be concluded that mixed restraint provides the most favorable ductility performance, followed by steel tube restraint, with actively restrained concrete outperforming unrestrained concrete. These findings robustly demonstrate that mixed restraint not only enhances the bearing capacity of concrete but also significantly improves its deformation capacity.

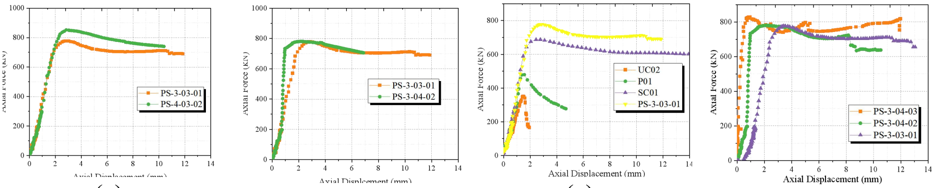

(a) (b) (c) (d)

Fig. 3. Specimen load - vertical displacement curve(a)different hoop-spacing (b)prestress levels (c)constraint forms (d)mixed constraint

3.2 Load-vertical strain and load- steel hoop strain analysis

The load-vertical strain curves for different constraint types are compared in Fig. 4. Strain data from the four groups of strain flower specimens were averaged, and only data within the strain gauge useful range (up to 20000με) were considered, excluding values above this threshold. The peak strain observed in unconstrained concrete was approximately 2000με. In contrast, prestressed steel hoop actively restrained concrete exhibited a peak strain of 8790με, while the maximum strain for the prestressed steel hoop itself was limited to 1350με. Prior to reaching yield point, excessive cracking deformation led to specimen failure. At a load reduction of 95% of its bearing capacity, the vertical strain reached 18850με. For specimen PS-3-03, when its load was reduced to 82% of its bearing capacity, it experienced a peak strain of 18,667 με; similarly for specimen PS-4-03 at a load reduction to 89% of its bearing capacity with a peak strain value recorded as18160με.

4 Numerical modeling

4.1 Material constitutive model

This finite element model adopts the stainless steel constitutive model proposed by Rasmusse KJR[14], as shown below:

$$\varepsilon = \frac{\sigma}{E_0} + 0.002\left(\frac{\sigma}{\sigma_{0.2}}\right)^n \quad (\sigma \le \sigma_{0.2}) \tag{1}$$

$$\varepsilon = \frac{\sigma - \sigma_{0.2}}{E_{0.2}} + \varepsilon_u\left(\frac{\sigma - \sigma_{0.2}}{\sigma_u - \sigma_{0.2}}\right)^m \quad (\sigma > \sigma_{0.2}) \tag{2}$$

Where: ε is the stainless steel strain; σ is the stainless steel stress; E_0 is the initial elastic modulus of stainless steel; $\sigma_{0.2}$ is the nominal yield strength of stainless steel and the corresponding stress at the residual strain 0.002; n is the strain hardening index, $n = \dfrac{\ln(20)}{\ln(\sigma_{0.2}/\sigma_{0.01})}$, $\sigma_{0.01}$ is the corresponding stress when the participating strain is 0.001, $E_{0.2}$ is the elastic modulus corresponding to the nominal yield point, and the ultimate strain of ε_u stainless steel. σ_u is the ultimate strength of stainless steel; m is coefficient, $m = 1 + 3.5\dfrac{\sigma_{0.2}}{E_0}$.

The plastic damage model is adopted for concrete, and the σ-ε model under pressure is adopted the concrete constitutive model proposed by Han Linhai [15], which considers the restraint effect of steel tube.

4.2 Contact setting

The interface model between the stainless steel plate and the core concrete consists of normal contact and tangential bond slip. The normal contact model between the stainless steel plate and core condensate adopts a "hard contact" approach, allowing complete transfer of pressure perpendicular to the interface, thereby enabling separation between the steel plate and the concrete during loading. For tangential contact, a Coulomb friction model is employed, facilitating shear stress transfer across the interface. When the shear stress reaches its critical value, relative sliding occurs with an interface friction coefficient of μ=0.3.

4.3 Initial prestress setting of prestressed steel hoops

The initial prestress of the prestressed steel hoops is established through the cooling method. When defining material properties, the linear expansion coefficient of stainless steel hoops is provided first, followed by defining the initial prestressed field temperature as 0. Subsequently, the temperature value corresponding to the initial stress is determined using the formula $\Delta T=\sigma/E\alpha$ in order to define the temperature reduction in prestressing field 1.

4.4 Element type selection, mesh division and boundary conditions

The stainless steel tube and the stainless steel hoop are shell units (S4) in a four-node fully integrated format. The core concrete adopts three dimensional solid unit (C3D8R) in the form of eight node reduction integral. The boundary conditions calculated in this paper are to impose fixed boundary conditions on the bottom end of the member, constrain all degrees of freedom except the axial displacement on the top of the specimen, and apply the axial displacement by setting the reference point coupled to the member. The grid division and boundary conditions of the model are shown in Fig. 5.

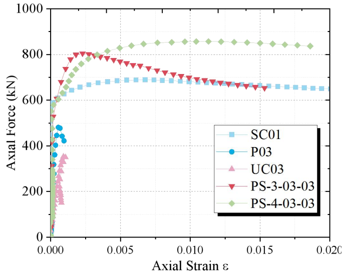

Fig.4. Axial force-axial strain curves of different constrained

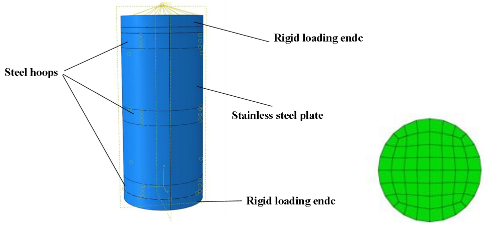

Fig.5. A schematic drawing of finite element model

5 Finite element model verification

5.1 Failure pattern

The aforementioned finite element model was utilized to validate the test specimens of prestressed steel hoop-steel tube mixed restraint concrete. Fig. 6 illustrates a comparison between the destruction patterns of SC, PS-3-03, PS-3-04 and PS-4-03 specimens in the finite element model and those observed in the actual test specimens. It is evident that both simulated and tested specimens experienced severe damage and significant buckling at their midsections, resulting primarily from waist drum type failure. However, due to less constraint caused by fine sand leveling at its lower part, the actual test specimen exhibited more pronounced drum bending than its upper part did, which is consistent with our damage comparison analysis.

(a) SC (b)PS-3-03 (c)PS-3-04 (d)PS-4-03

Fig.6. Comparison of damage modes between ABAQUS model and test specimens

5.2 Comparative analysis of load-displacement curve and bearing capacity

The comparison between the test results and the simulation results of the load-strain curves of the specimens is illustrated in Fig. 7. It can be inferred that, overall, there is a good agreement between the two sets of data, with similar stiffness observed in the elastic segments and a relatively gentle decline in strain after reaching peak point, indicating favorable ductility. This phenomenon can be attributed to stainless steel material's pronounced strain strengthening performance post-yielding, resulting in stronger restraint on core concrete once member's elastic stage concludes. From Table 3, it can be deduced that while the simulated results exhibit higher bearing capacity values compared to those obtained from testing, they still follow a consistent pattern. The potential reasons for this disparity may include: (1) The presence of uniformly distributed fine sand at the bottom of the test setup reduces constraint effects on specimen's base and leads to concrete crushing; thus resulting in lower bearing capacity than what was simulated. (2) In contrast to actual tests where prestressed steel hoops are connected using bolts, simulations employ integral prestressed steel strips. During later stages of loading, slippage may occur among bolts securing middle section's prestressed steel hoop which diminishes its restraining effect and consequently lowers bearing capacity relative to simulation.

Table 3. Comparison of bearing capacity between ABAQUS model and test specimens

Specimen	Number	Test N_0	Average value $N_{0\mu}$	FE model N_u	$N_{0\mu}/N_u$
	PS-3-03-01	777.700			
PS-3-03	PS-3-03-02	743.400	775.1	801.96	0.9665
	PS-3-03-03	804.230			
	PS-3-04-01	871.600			
PS-3-04	PS-3-04-02	780.500	814.8	937.41	0.8692
	PS-3-04-03	792.200			
	PS-4-03-01	861.700			
PS-4-03	PS-4-03-02	853.400	857.5	970.65	0.8833
	PS-4-03-03	857.400			
	SC01	688.6			
SC	SC02	694.5	688.6	747.31	0.8947
	SC03	682.8			
	P01	494.3			
P	P02	520.7	482.3	538.08	0.8963
	P03	504.4			

6 Conclusion

(1)The mixed constrained concrete column effectively restrains the specimens during the initial loading stage, thereby avoiding the stress hysteretic problem associated with passive constraint. Additionally, it significantly enhances the axial compression capacity of the steel plate constraint specimen. As the space between prestressed steel hoops decreases and the initial prestress level increases, there is a corresponding increase in bearing capacity. Notably, reducing the space between prestressed steel hoops has a more pronounced effect on improving bearing capacity.

(2) The mixed constrained concrete column effectively enhances the deformation performance of the specimen, exhibiting significantly improved ductility compared to prestressed steel hoop-constrained and steel pipe restrained members.

(3) Based on the FE model, the calculated results demonstrate good agreement with operational results. It is confirmed that the presence of the fine sand causes larger deformations at the lower part of the specimen.

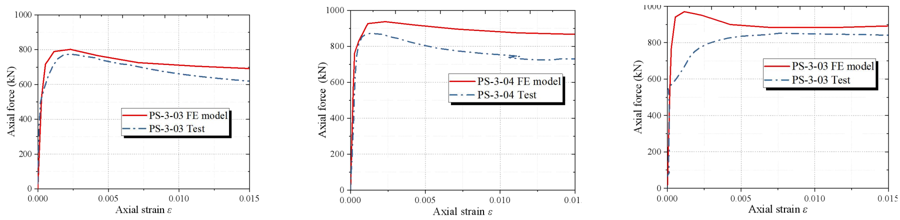

Fig.7. Comparison of axial force-axial strain between model and test specimens

Acknowledgement

The work was supported in part by the National Natural Science Foundation of China (52408253), the Science and technology research project of colleges and universities in Hebei Province (QN2023002) and Natural Science Foundation of Hebei (No. E2023202237).

References

[1]. Shin M, Andrawes B. Experimental investigation of actively confined concrete using shape memory alloys. Engineering Structures 32: 656-64 (2010).
[2]. Lin H J, Liao C I. Compressive strength of reinforced concrete column confined by composite material [J]. Composite Structures 65(2):239-250 (2004).
[3]. Schneider S P. Axially loaded concrete-filled steel tubes. Journal of Structural Engineering, ASCE, 1998, 124(10):1125-1138.
[4]. Wang Yuyin. Research on basic performance of circular steel tubular high-strength concrete axial compression short column. Harbin Institute of Technology, (2003).
[5]. Sun Yue, Zhu Weiqing, Jia Jinqing, et,al. Failure modes and deformation characteristics of steel reinforced high-strength concrete columns. Journal of Inner Mongolia University of Technology (Natural Science Edition), 2024, 43(04): 351-359.
[6]. Gao Wencai. Axial behavior of stainless steel tube confined concrete short columns with circular cross-section. [D]. Harbin Institute of Technology, 2016.
[7]. Chai Y H, Priestley M J N, Seible F. Seismic retrofit of circular bridge columns for enhanced flexural performance [J]. ACI Structural Journal 88(5): 572-584 (1991).
[8]. Huang Y, Xiao J, Zhang C. Theoretical study on mechanical behavior of steel confined recycled aggregate concrete. Journal of Constructional Steel Research 76: 100-111 (2012).
[9]. Choi E, Kim D, Park K. Effect of Confining Pressure Due to External Jacket of Steel Plate or Shape Memory Alloy Wire on Bond Behavior Between Concrete and Steel Reinforcing Bars. Journal of Nanoscience and Nanotechnology 14(12):9657-9661 (2014).
[10]. Saatcioglu M, Yalcin C. External Prestressing Concrete Columns for Improved Seismic Shear Resistance [J]. Journal of Structural Engineering 129(8): 1057-1070 (2003).

[11]. Fakharifar M, Chen G, Wu C, et al. Rapid Repair of Earthquake Damaged RC Columns with Prestressed Steel Jackets. Journal of Bridge Engineering 21(4) (2016).
[12]. GB/T228.1-2010 Metallic materials-Tensile testing - Part 1: Method of test at room temperature. China Standard Press, (2012).
[13]. GBT 50152-2012 Standard for test method of concrete structures. China Building Industry Press, (2003).
[14]. Rasmussen K J R. Reply to: Discussion of Full-range stress-strain curves for stainless steel alloys. Journal of Constructional Steel Research 59(10): 1325-1326 (2003).
[15]. Han Linhai. Concrete filled steel tubular structures -Theory and Practices. [M]. Beijing: Science Press, (2004).